ELSEVIER

Journal of Structural Geology 27 (2005) 1113–1127

JOURNAL OF STRUCTURAL GEOLOGY

www.elsevier.com/locate/jsg

Analysis of the relationships between strain, polarity and population slope for normal fault systems

Shunji Moriya[1], Conrad Childs*, Tom Manzocchi, John J. Walsh

Fault Analysis Group, Department of Geology, University College Dublin, Dublin 4, Ireland

Received 28 May 2003; received in revised form 4 January 2005; accepted 20 January 2005
Available online 29 June 2005

Abstract

The evolution of normal fault populations and their synthetic and antithetic sub-populations has been studied for a number of fault systems imaged from seismic reflection data. Relationships between fault strain and polarity and the slope of fault throw populations have been investigated by backstripping a fault system in the Inner Moray Firth, North Sea, and by comparison between throw populations for pre-faulting horizons from an additional 11 fault systems with variable extensional strains. Fault population slopes decrease with increasing strain reflecting strain localisation onto progressively fewer and larger faults. Synthetic and antithetic sub-populations also show an inverse relationship between slope and the strain they accommodate, but the slopes of antithetic sub-populations are independent of the total strain on the fault system. The slopes of antithetic sub-populations are higher than those of synthetic sub-populations from the same area and the difference in slope correlates with the polarity of the fault system, i.e. the proportion of the total strain accommodated by the two sub-populations. The data are consistent with progressive decrease in the slopes of sub-populations until the antithetic fault sets become inactive. The absence of a correlation between strain and polarity is attributed to the effects of fault system reactivation.

Keywords: Strain localisation; Polarity; Fault populations; Reactivation

1. Introduction

1.1. Fault populations

Size distributions (displacements or lengths) of tectonic faults are generally characterised by a power-law scaling relationship (Kakimi, 1980; Childs et al., 1990; Scholz and Cowie, 1990; Walsh et al., 1991). Power-law fault size populations are investigated on a log–log plot of cumulative frequency (N) versus fault size (S)

$$\log(N) = c - M\log(S) \quad (1)$$

where c is a constant and M is the power-law exponent or slope on the cumulative frequency plot. Size populations can be defined by 1D, 2D and 3D samples of the faulted rock volume. In practice, fault populations are derived from 1D line samples (e.g. offsets of a horizon on a seismic line) or 2D map samples. In this paper we present both 1D and 2D samples of fault throw and we denote the derived 1D and 2D power-law exponents as m_1 and m, respectively. Because not all fault traces are sampled on 1D line samples across a map, there is a systematic under-representation of small faults on 1D samples compared with 2D samples, so that the different sample domains result in different power-law exponents. The difference between m_1 and m is given by $m = m_1 + 1/n$ (Marrett and Allmendinger, 1991) where n is the exponent relating maximum fault displacement (D) to length (L) in the relationship $D \propto L^n$. Empirical values of n are generally in the range 1–2 (Ranalli, 1977; Walsh and Watterson, 1988; Marrett and Allmendinger, 1991; Walsh et al., 1991; Dawers and Anders, 1995; Schlische et al., 1996).

Systematic variations in fault size distributions during fault system evolution have been predicted from physical experiments (Ishikawa and Otsuki, 1995) and numerical models (Cowie et al., 1995; Cladouhos and Marrett, 1996; Cowie, 1998). The evolution of faults within these numerical models is characterised by a progressive decrease in the power-law exponent with increasing strain, which is

* Corresponding author. Tel.: +353 1 716 2608; fax: +353 1 716 2607.
E-mail address: conrad@fag.ucd.ie (C. Childs).
[1] Present address: JAPEX, NYK Tennoz Building 21F, 2-2-20 Higashi-Shinagawa, Tokyo 140-0002, Japan.

0191-8141/$ - see front matter © 2005 Elsevier Ltd. All rights reserved.
doi:10.1016/j.jsg.2005.01.017

indicative of progressive strain localisation onto larger faults. These numerical models are consistent with observations that fault populations that accommodate large strains typically have relatively shallow population slopes (Kakimi, 1980; Marrett and Allmendinger, 1992; Wojtal, 1994, 1996). Kinematic analyses of fault population evolution based on geological data have only recently been published. Meyer et al. (2002) have shown that the power-law exponent for lengths and geometric moments of faults in an area of low strain (ca. 4%) in the Timor Sea decreased during extension, although the exponent for throw remained constant. Walsh et al. (2003) demonstrated that localisation of strain during growth of a fault system in the Inner Moray Firth, offshore UK was also accompanied by a decrease in slope, reflecting a change in the character of the length population from a power-law distribution at early times to a power-law distribution with a marked non-power-law tail at large lengths. Here, we present the results of fault throw population analysis for the area of the Inner Moray Firth that has previously been analysed for fault length by Walsh et al (2003). We are not concerned with the detailed character of individual population curves and the possible reasons for departures from a perfect power-law population. Instead we are interested in the relative numbers of large and small faults within a population as indicated by the overall slope of the population curve.

The Inner Moray Firth study area is unusual in that the rate of sedimentation exceeded fault displacement rates so that the faults were continuously blanketed during extension. Under these conditions fault growth histories are recorded in across-fault sediment thickness changes allowing restoration of fault displacements through time. In the majority of extensional basins sedimentation rates are low in relation to fault displacement rates, precluding accurate restoration of fault growth histories. In such areas, however, it is generally possible to derive accurate present day fault populations from seismic mapping of pre-faulting horizons. Here, we describe the temporal variation in restored m and m_1 with increasing strain in the Inner Moray Firth study area, and compare this with variations in m values for 11 other areas of different strain. To assist this comparison, we present both present day and restored throw populations for the Moray Firth area derived from both 1D and 2D samples. The reasons for choosing different sample domains for the two elements of our study are described in the relevant sections.

1.2. Fault system polarity

The polarisation of fault systems, into dominant (synthetic) and subordinate (antithetic) fault dip directions, has been studied almost exclusively in the context of gravity driven structures (Stewart and Argent, 2000 and references therein) formed in response to regional tilting or removal of a ‘sidewall buttress’ by, for instance, incision of a river channel or fault scarp formation. In these systems, the dominant dip direction of polarised fault systems is thought to be controlled primarily by the mechanical properties of the faulted sequence. Where a discrete detachment defines the base of the faulted interval the faults tend to dip downslope while they dip upslope in the absence of such a detachment (Higgs and McClay, 1993; Stewart and Argent, 2000). The polarisation of tectonic normal fault systems has not, to our knowledge, been studied in any detail (but see Kakimi (1980)). It is generally observed that in areas of high strain, large faults tend to dip towards the centre of a graben or half-graben (e.g. the Gullfaks Oilfield; Fossen and Hesthammer, 1998) while in areas of low tectonic strain there may be no dominant sense of fault dip (e.g. British Coalfield; Watterson et al., 1996). During the evolution of tectonic fault systems, therefore, faults might be expected to become progressively polarised towards a dominant dip direction, which should be reflected in fault population systematics. Kakimi (1980) predicted not only that the power-law exponent for fault throw populations should decrease with fault maturity but also demonstrated that the exponent for the dominant, or synthetic, fault dip direction is lower than that of the antithetic dip direction. Here, we examine changes in the slopes of synthetic and antithetic sub-populations through time for the Moray Firth area and also variations in slope between areas that have undergone different extensional strains. We examine relationships between the difference in slope of the two sub-populations and fault system polarity, total strain and the strain accommodated on the individual dip sets. Although our study is primarily for tectonic faults we also include one dataset from a gravity driven fault system formed above a salt detachment.

Strain (ε) is calculated here as the sum of the geometric moments (Scholz and Cowie, 1990) of all the interpreted faults on a mapped horizon, divided by the horizon area (A)

$$\varepsilon = \frac{1}{A}\sum_{n=1}^{N} LD \tag{2}$$

where N is the total number of faults, and D and L are average displacement and length, respectively, of individual faults. This measure of strain is adopted for both 2D and 1D multi-line population sampling schemes. Polarity or the degree of polarisation (P) is defined as:

$$P = \frac{\varepsilon_s - \varepsilon_a}{\varepsilon_t} \tag{3}$$

where ε_t is the total strain and ε_s and ε_a are the strain accommodated by the synthetic and antithetic faults, respectively. In this article, synthetic faults refer to faults that dip in the same direction as the largest fault in the area studied. As defined here, P can range from close to -1, for a system strongly polarised to the antithetic fault direction, to 1 for a system entirely polarised in the synthetic fault direction. In practice P will usually be positive, i.e. the higher strain fault set will contain the largest fault. In one

low polarity fault system studied here, the direction of polarisation is different on two horizons at different structural levels so that a low negative polarity is recorded on one. In this article we firstly describe the evolution of the Moray Firth study area in terms of temporal variations in strain, population slope and polarity. For the other temporal evolution was not studied, but their range of present-day strains allowed examination of the variation in population slope and polarity with strain.

2. Evolution of a fault throw population from the Inner Moray Firth

2.1. Backstripping of throw populations through time

The Inner Moray Firth study area (Fig. 1, Table 1), is covered by a 15×6.5 km seismic survey with seismic lines spaced every 100 m; this seismic dataset also formed the basis for an earlier study on fault length populations (Walsh et al., 2003). During the Late Jurassic the area underwent 16 My of rifting (Underhill, 1991a,b) along NE–SW striking normal faults with throws up to 450 m within the study area. Syn- and post-rift sequences up to 3 km thick preserve the complete faulting history so that the evolution of the fault system can be reconstructed using the displacement (or throw) backstripping method described by Petersen et al. (1992) and Childs et al. (1993). The backstripping method involves the subtraction of fault throws on syn-faulting horizons from those on an underlying, usually top pre-rift, horizon, to give the throws on the older horizon at the time of deposition of the younger horizons. The main requirement of the method is that the sedimentation rate exceeded the fault displacement rate. The validity of application of the throw backstripping method applied to this area is discussed in detail in Walsh et al. (2003). The fault array mapped on a pre-rift horizon (Horizon TT, Fig. 1a) has been backstripped to the time of deposition of five overlying syn-rift horizons (Fig. 1b, Table 1) providing fault throw populations for six time steps

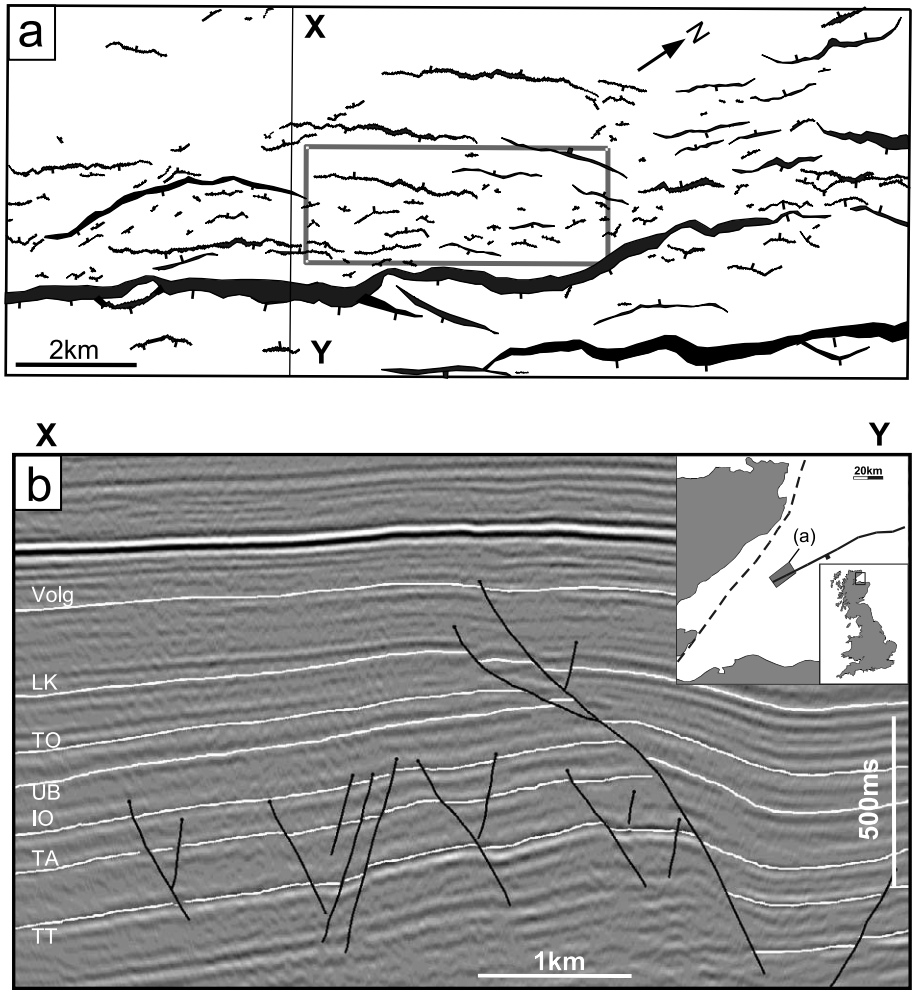

Fig. 1. Fault map for Horizon TT (a) and seismic line (b) from the Inner Moray Firth, UK North Sea. The sub-area outlined in (a) is discussed in the text. The horizon labels on the left of (b) are for the pre-faulting horizons (TT and TA) and the younger horizons within the growth sequence used in displacement backstripping. The location of the map in (a) is shown in the inset to (b).

Table 1
Parameters and throw population data for the Moray Firth dataset derived from 1D multiline sampling

Horizon	Max throw (m)	Strain	Polarity	m_1	m_{1s}	m_{1a}
TT(IO)	170	0.028	0.48	0.95 (0.85–1.06)	0.72 (0.63–0.80)	1.12 (1.06–1.66)
TT(UB)	319	0.058	0.60	0.72 (0.67–0.77)	0.51 (0.48–0.55)	0.96 (0.90–1.17)
TT(TO)	416	0.072	0.67	0.66 (0.62–0.70)	0.47 (0.44–0.50)	0.96 (0.90–1.14)
TT(LK)	442	0.082	0.71	0.64 (0.59–0.67)	0.44 (0.43–0.47)	0.96 (0.92–1.14)
TT(Volg)	462	0.091	0.73	0.61 (0.58–0.64)	0.42 (0.40–0.43)	0.96 (0.92–1.14)
TT (present)	462	0.093	0.74	0.60 (0.58–0.64)	0.41 (0.39–0.42)	0.96 (0.88–1.13)

The data are for the TT horizon at the present day and backstripped to the time of deposition of younger horizons (names in brackets). m_1 is the total population slope and m_{1a} and m_{1s} are the slopes of the antithetic and synthetic populations, respectively.

including the present-day (Fig. 2a). In addition, the restored fault populations were divided into synthetic (SE dipping) and antithetic (NW dipping) sub-populations (Fig. 2b and c).

The restored fault populations are derived for 1D multi-line samples of the map area. 1D multi-line samples are constructed from multiple, usually parallel, transects across a map area. The throw is recorded where a sample line intersects a fault trace and the population comprises the throw measurements for all sample-lines (Childs et al., 1990); for seismic datasets the sample lines are, in practice, the seismic shotlines, which are ideally oriented normal to fault strike. The throw data are plotted on a log–log graph of throw vs. the cumulative number of measurements with higher throws (e.g. Fig. 2a). The slope of the straight-line portion of the resultant curve is the 1D power-law exponent m_1 (see Eq. (1)). The construction of restored fault populations from 2D populations is more subjective than the 1D approach. The construction of 2D backstripped populations requires not only that the fault throws are backstripped through time, but also that faults which grew in length by segment linkage are restored to their pre-linkage geometries. For fault systems imaged on seismic data the limit of lateral resolution of the data precludes identification of all of the sites of segment linkage that introduces an uncertainty in the backstripped 2D population not associated with 1D samples. Nevertheless we later present the 2D population of the pre-rift horizon (TT) restored to the time of deposition of the first mapped syn-faulting horizon (Fig. 2d) and show that the changes in 2D populations are in agreement with the better defined changes for 1D populations.

The 1D fault populations for the pre-rift TT Horizon at different stages of growth of the fault system are shown in Fig. 2a. All size populations derived from seismic data are subject to a lower limit of resolution imposed by the throw resolution of the seismic data, below which the slope of the population curve departs from a straight line. 1D multi-line samples also depart from a straight line at the upper throw range due to multiple sampling of individual faults having trace lengths longer than the spacing between seismic lines. Where the sampled faults extend across the entire survey area the curve departs from a straight line at a cumulative number equal to the number of sample lines, e.g. 150 sample lines is appropriate to Fig. 2a. Where faults do not extend across the area, this cutoff is lower, such that the power-law exponent for the antithetic fault population (Fig. 2c) is determined for cumulative numbers greater than ca. 70

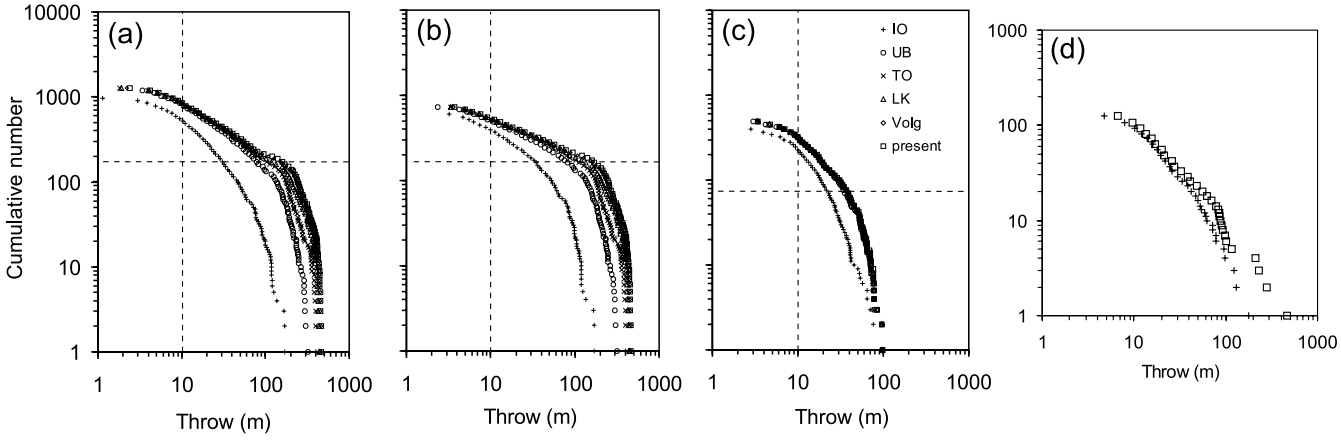

Fig. 2. (a)–(c) 1D multi-line fault throw population curves for the present day TT Horizon and the TT Horizon backstripped to the time of deposition of five younger horizons, for (a) all faults, (b) synthetic faults and (c) antithetic faults. The cumulative number of measurements defining the limit of significant data (horizontal dashed line) is different for the synthetic and antithetic populations as discussed in the text. The throw resolution for the seismic dataset is 10 m. The slopes and estimated ranges of slope for the curves in (a)–(c) are shown in Fig. 3. (d) 2D maximum fault throw populations for the present day TT Horizon and the TT Horizon backstripped to the time of deposition of the IO Horizon. The estimated slope for the backstripped horizon is 1.9 and lies within the range 1.5–2.1. The key in (c) applies to each figure.

rather than the total number of 150 seismic lines. The significant portion of 1D population curves from which the power-law exponent is derived lies between these upper and lower bounds (Childs et al., 1990; Walsh et al., 1994; Yielding et al., 1996). Within these limits, the present day and restored population curves define approximately straight power-law relationships. Population slopes were measured by fitting manually a best-fit line through the relevant part of the population curve. Errors associated with slope measurements were estimated by fitting what is considered to be the maximum and minimum slopes that could reasonably be drawn through the relevant part of the population curve.

2.2. Strain localisation

The slope of the 1D throw population curve for all faults in the study area (Fig. 2a) progressively decreases with increasing strain (Fig. 3). This decrease indicates that the proportion of extension accommodated by large faults increases as the fault system evolves and strain is increasingly localised onto larger faults. These conclusions based on throw population analyses are consistent with those reached from length population analyses of the same area by Walsh et al. (2003).

The number of throw measurements derived from the multi-line sampling of a horizon is a proxy for the mapped fault length on that horizon. For the Inner Moray Firth data each measurement represents a fault length that is at least equal to the sample line spacing of 100 m. The increase in cumulative number of throw measurements between the time of deposition of the IO and UB horizons (Fig. 2a) therefore indicates an increase in total fault length during this time interval. The total number of measurements for the UB and younger horizons is approximately constant and, therefore, the total fault length did not increase significantly following the deposition of UB. The restored throw populations are constructed for the pre-faulting TT horizon so that a backstripped population includes both the faults that were dead and active at any particular time. The proportion of dead faults within the population, however, increased through time. Inspection of seismic lines (e.g. Fig. 1b) indicates that the majority of small faults do not extend for significant distances above the IO horizon so that populations for later deposited horizons comprise predominantly dead faults. Strain localisation and the progressive decrease in m_1 through time is therefore primarily due to the death of small faults as described by Walsh et al. (2003).

2.3. Polarisation

As with the total fault population, the population of synthetic faults shows a progressive decrease in population slope with increasing strain (Fig. 3) from a slope of ca. 0.75 at the time of deposition of the IO horizon (strain ca. 0.028) to 0.4 at the present day (strain ca. 0.09). In contrast, there is very little change in the character of the antithetic population following deposition of the UB horizon (strain = 0.06) and an initial, poorly defined, population slope of ca. 1.1 decreases only slightly to a constant value (0.95) at higher strains. The population of antithetic faults was effectively dead before deposition of the UB horizon as seen in cross-section (Fig. 1b) where none of the antithetic faults intersect this horizon. During the subsequent evolution of the fault population only the synthetic, southeast dipping faults were active, so there was a systematic increase in both the polarity of the fault system and the difference in slope of the synthetic and antithetic populations (Fig. 4). When the data trends for polarity and difference in slope are extrapolated to zero strain they do not pass through the origin but intersect the y-axis in Fig. 4, at

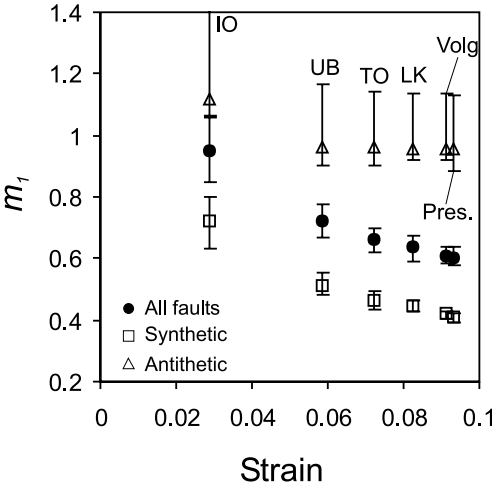

Fig. 3. 1D throw population slope (m_1) vs. strain for the backstripped TT horizon. The bars on each point show errors in the slope estimated by fitting the highest and lowest slope that can reasonably be fitted to the straight line portion of the population curve.

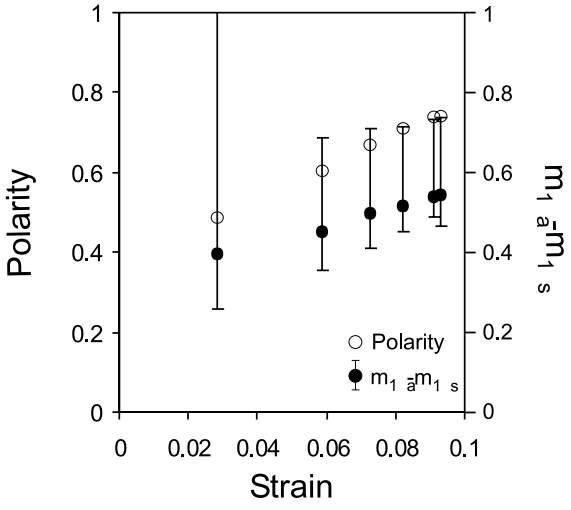

Fig. 4. Polarity (open circles) and difference in slope (solid circles) of synthetic and antithetic throw populations (m_{1a}–m_{1s}) against strain for the backstripped TT Horizon. Error bars are attached to the m_{1a}–m_{1s} estimates.

0.4 and 0.3, respectively. These observations are interpreted to indicate that the fault system was either polarised from the onset of extension or alternatively became polarised rapidly at strains less than 0.028. Early polarisation of the fault system might occur if the synthetic faults reactivated earlier formed basement structures. Jurassic reactivation of pre-existing, possibly Permo-Triassic, faults in the Inner Moray Firth has been suggested by Underhill (1991a,b) but there is no direct evidence of basement faulting in the seismic survey studied here.

The difference in evolution of the synthetic and antithetic fault populations is further illustrated by comparison between the present day 1D (Fig. 2a–c) and 2D (Fig. 5, NS1) samples of the two fault dip directions. The cumulative number of measurements for 1D samples reflects the total fault length in the study area. As the spacing between adjacent sample lines (seismic shotlines) is 100 m and the faults strike normal to the sample line orientation, each measurement represents about 100 m of fault length. The total number of throw measurements greater than 10 m (the throw resolution of the seismic data) for the synthetic population is ca. 500, representing a total fault length of 50 km. For the antithetic population the total number of readings is 300, implying a total fault length of 30 km. If, on the other hand, we compare the 2D populations, which record each fault as a single datum on the cumulative frequency plot, there are ca. 60 antithetic faults but only 30 synthetic faults. This reversal in the total cumulative number of antithetic and synthetic faults reflects different degrees of maturity of the two fault sets. The synthetic faults grew for a longer period of time and initially unconnected fault segments linked together resulting in progressively fewer and longer individual faults, as described by the model of Walsh et al. (2003). The antithetic faults, however, became inactive early in the growth of the fault system preserving a more immature fault system containing a greater number of smaller faults.

The larger total length of synthetic faults, together with the early formation of most faults, could be taken as evidence that the total synthetic fault length was always

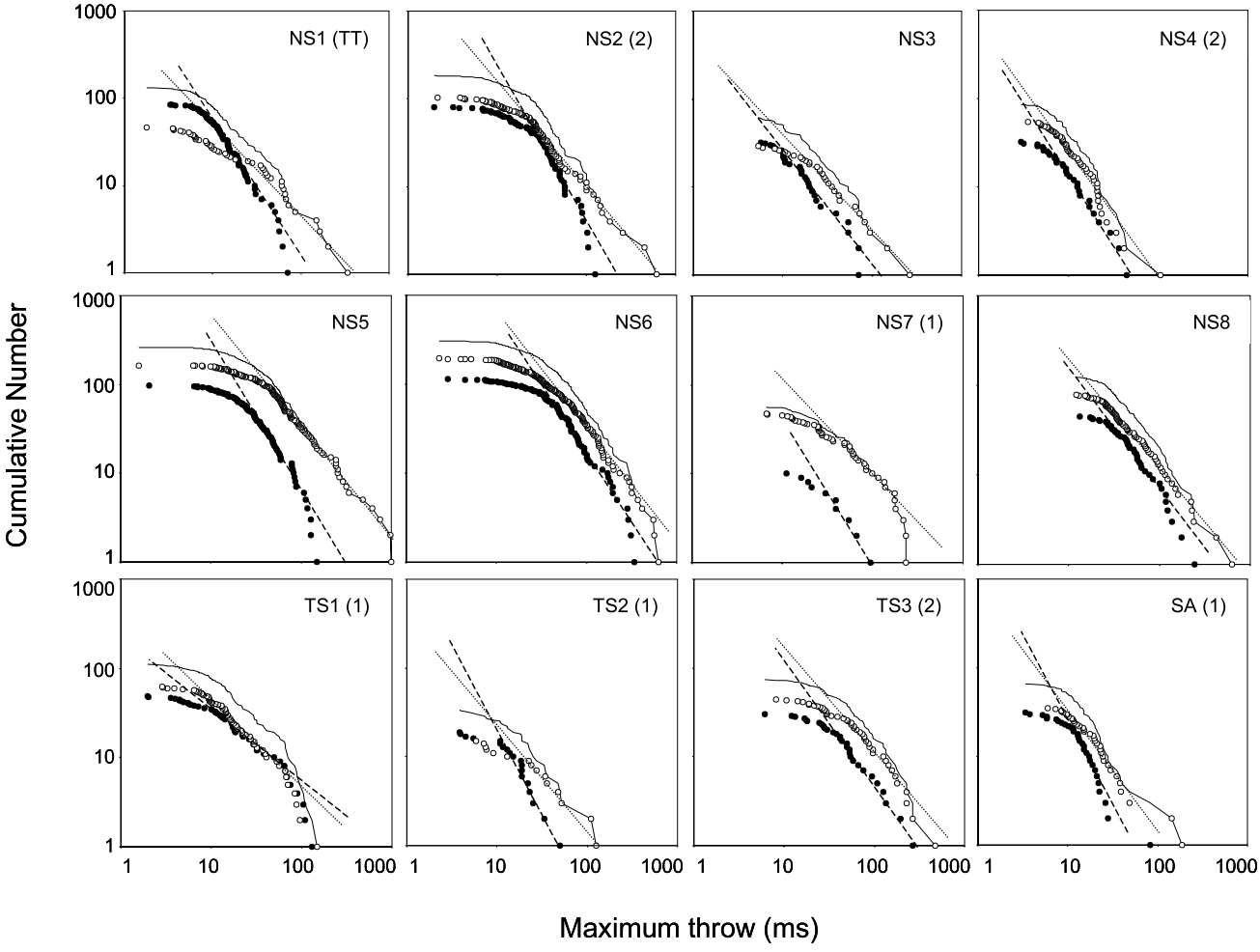

Fig. 5. Maximum throw population curves (2D samples) for one horizon from each of the 12 analysed datasets (see Table 2); horizon labels are given in parentheses after the dataset label. Each plot shows the curve for the entire fault population of mapped faults (solid line) and its synthetic (open circles) and antithetic sub-populations (filled circles). Best fit lines to the synthetic (dotted) and antithetic (dashed) populations are also shown. Throws are in milliseconds but can be converted to metres using ratios that can be derived from the maximum throws listed in Table 2.

greater than the antithetic length and the synthetic fault set dominated from the onset of extension. However, this may not be the case. The cumulative numbers of measurements for the 1D populations described above are taken at the lower limit of seismic resolution, i.e. 10 m. Extrapolations of the straight line portions of the present day synthetic and antithetic populations to lower throws converge, so that the cumulative numbers of measurements for the synthetic and antithetic populations would be the same (ca. 700) at a throw of 5 m. Extrapolated to throws lower than 5 m the total length of antithetic faults would be greater than that of the synthetic faults. It is therefore not possible to establish which, if either, of the two sub-populations dominated in terms of length at the onset of extension on the basis of the throw populations.

In summary, the fault throw populations for the Inner Moray Firth demonstrate localisation of strain onto progressively fewer and larger faults. Preferred localisation of strain onto synthetic faults is reflected in a lower population slope than that of the antithetic faults that died early in the growth of the fault system. The synthetic fault set had become dominant by the time of deposition of the first mapped syn-rift horizon at a strain of 0.028. Within the time resolution of the data it is not possible to determine whether the fault system was polarised from the onset of extension due to reactivation of basement faults or from an initially symmetrical, non-reactivated fault system during an initial strain of ~0.03, representing one third of the total strain.

3. Strain localisation and polarisation of other normal fault systems

Displacement backstripping of the Inner Moray Firth dataset illustrates a systematic change in the fault population through time arising from the progressive localisation and polarisation of the fault system. The geological conditions required to perform displacement backstripping are, however, rare. More commonly the rate of syn-faulting sedimentation is significantly lower than the fault displacement rate so that the syn-rift thickness variations do not record fault displacement distributions through time. Nevertheless, a pre-faulting horizon that is unaffected by erosion records the final throw population. By comparing throw populations from areas with different strain magnitudes we can investigate whether the strain-related trends observed in the Inner Moray Firth are applicable to fault systems in general. In this section we describe the results of population analyses on 23 pre-faulting horizons from 12 areas (Fig. 5) in the North Sea (including the Inner Moray Firth), offshore South America and the Timor Sea, offshore NW Australia; one of the NW Australia datasets (TS1) formed the basis for a previous study of fault population evolution (Meyer et al., 2002). More than one horizon has been included for analysis for selected datasets to give an indication of the variability between individual horizons and, in areas of reactivation, to illustrate the differences in populations for horizons that have undergone one and two phases of extension. Representative throw populations and the synthetic and antithetic sub-populations for each area are shown in Fig. 5. Examples of seismic lines across three of the data volumes are shown in Fig. 6 and details of the datasets are given in Table 2. The seismic datasets are 3D surveys apart from the NS2 dataset, which is a 2D survey comprising widely spaced (~1 km) seismic lines. The populations are, in general, well defined allowing a power-law exponent to be estimated with confidence. There are, however, certain populations for which the number of faults or the range of fault throws is low, for example the antithetic populations in NS7 and TS2. The population slopes have been determined by fitting manually a best fit line to the population curve over the adequately sampled throw range. This throw range is bounded at the lower end by the resolution of the seismic data while at the upper end the largest faults within a population are often under- or oversampled resulting in departures from a straight line distribution. The uncertainty in estimation of population slopes is expressed in the ranges attached to each population and sub-population (Table 2). Uncertainties associated with the measurement of 2D population slopes were estimated by fitting what is considered to be the maximum and minimum slopes that can be drawn through the adequately sampled part of the curve.

The populations used in this part of the study (Fig. 5) are from 2D, rather than 1D samples. While 1D populations are more reliably backstripped than 2D populations, 1D populations provide a less robust means for deriving m values for synthetic and antithetic populations. Subdividing populations into the synthetic and antithetic component sets by definition involves assigning the largest fault to the synthetic population, which could predispose the synthetic population to have a lower slope. This would have a pronounced effect on 1D multi-line sample populations in areas where many throw measurements derived from a single large fault dominate the throw population. For 2D samples, assigning the single maximum displacement value for the largest fault to one sub-population does not have a significant effect on the two component populations. As for 1D population samples, 2D samples are subject to the limits of seismic data resolution, but are affected to a lesser extent by non-power-law tails at high throw values (sampling effects on 2D populations are discussed by Pickering et al. (1995) and Walsh et al. (1994)).

3.1. Variations in population slope with strain and polarity

The variation in population and sub-population slopes for the combined datasets show similar patterns to that of the Inner Moray Firth dataset. There is a negative correlation between strain and population slope (Fig. 7a) that parallels

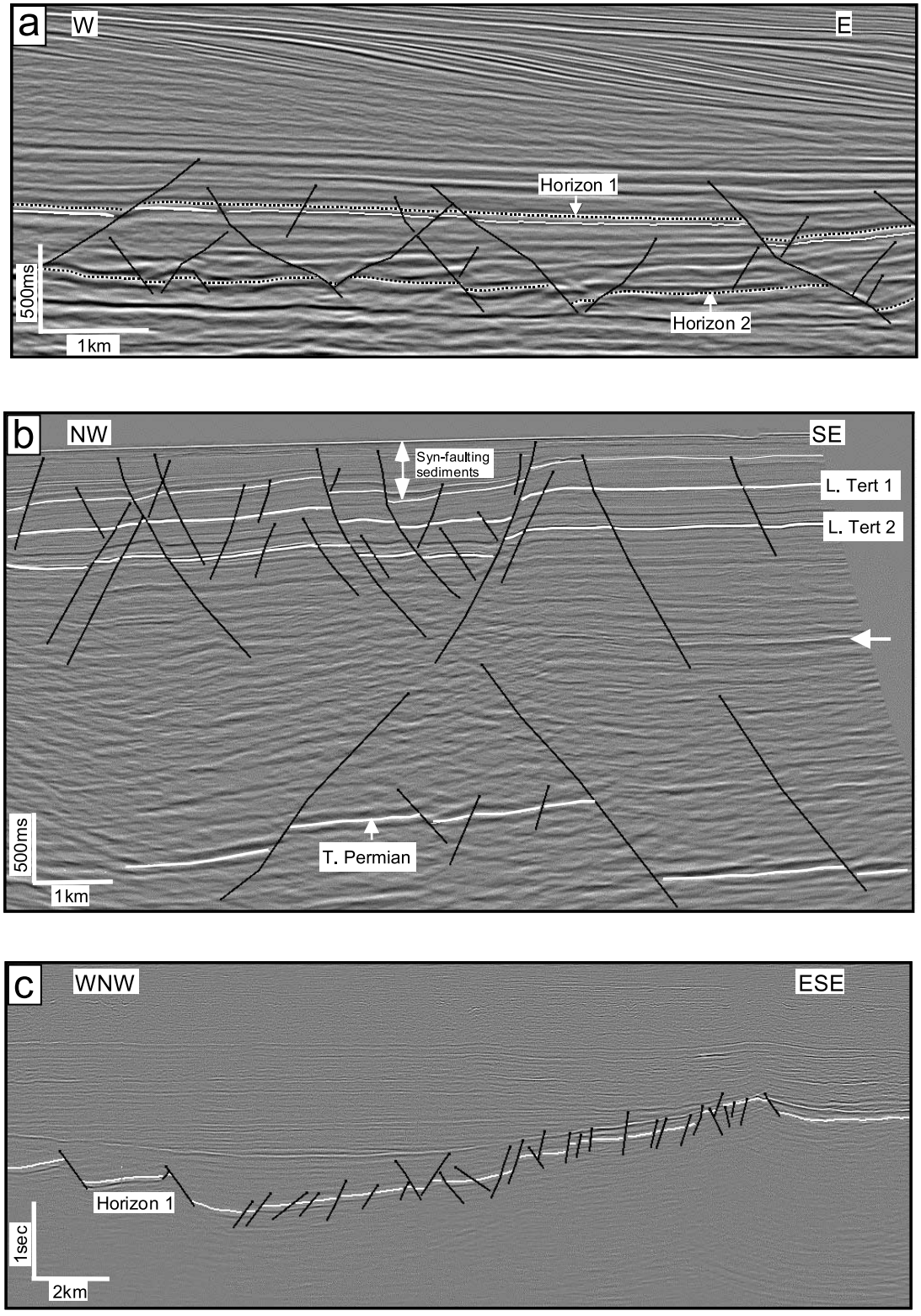

Fig. 6. Seismic sections normal to general fault strike through the (a) SA, (b) TS1 and (c) NS6 datasets (see Table 2 for further details). Interpreted horizons for which populations have been presented are labelled. The strong reflection that is on average 200 ms deeper than Horizon 2 in (a) is the base of a salt layer. The arrow on the right of (b) indicates the approximate level of an unconformity that truncates faults formed during an initial phase of Late Jurassic–Early Cretaceous extension. The lowest point on Horizon 1 in (c) is the floor of the Viking Graben as discussed in the text.

Table 2
Parameters and throw population data for the 12 datasets and 23 horizons analysed

Dataset	Horizon	Map area (km^2)	Number of faults	Max throw (ms)	Max throw (m)	Strain	Polarity	m	m_s	m_a
NS1	TA	93	125	342	470	0.10	0.72	1.16 (0.82–1.24)	0.96 (0.84–1.144)	1.55 (1.51–1.61)
	TT	93	134	335	462	0.09	0.74	1.18 (0.91–1.33)	1.04 (0.92–1.22)	1.56 (1.41–1.79)
NS2	1	1872	213	613	1808	0.05	0.57	1.54 (1.43–1.66)	1.33 (1.28–1.54)	1.69 (1.60–1.77)
	2	1872	184	615	1814	0.05	0.60	1.48 (1.46–1.60)	1.18 (1.18–1.24)	1.66 (1.66–1.73)
	3	1872	132	567	1673	0.05	0.62	1.47 (1.46–1.60)	1.21 (1.19–1.33)	1.61 (1.60–1.70)
NS3	1	111	61	261	384	0.05	0.54	1.18 (1.18–1.33)	1.07 (1.07–1.15)	1.29 (1.24–1.38)
NS4	1	58	85	167	209	0.04	0.49	1.40 (1.38–1.60)	1.19 (1.15–1.24)	1.54 (1.27–1.54)
	2	58	86	106	133	0.03	0.39	1.51 (1.50–1.66)	1.48 (1.40–1.60)	1.60 (1.60–1.66)
NS5	1	646	260	995	1358	0.12	0.77	1.36 (1.33–1.43)	1.23 (1.23–1.28)	1.65 (1.60–1.80)
NS6	1	870	308	629	1179	0.15	0.47	1.43 (1.37–1.49)	1.33 (1.27–1.39)	1.56 (1.42–1.64)
NS7	1	92	57	231	315	0.11	0.89	1.17 (1.02–1.38)	1.05 (0.97–1.11)	1.63 (1.48–1.73)
	2	104	61	200	273	0.13	0.90	1.36 (1.19–1.43)	1.20 (1.15–1.28)	1.77 (1.60–1.88)
NS8	1	357	123	635	749	0.11	0.45	1.40 (1.37–1.46)	1.20 (1.17–1.31)	1.36 (1.27–1.48)
TS1	L. Tert 1	112	111	147	221	0.08	−0.05	0.93 (0.88–0.98)	0.93 (0.87–1.15)	0.87 (0.82–0.89)
	L. Tert 2	131	96	149	224	0.07	0.11	0.91 (0.79–0.99)	0.83 (0.76–0.83)	0.90 (0.84–0.97)
	T. Perm	132	28	608	912	0.14	0.39	0.94 (0.87–1.03)	0.80 (0.73–0.96)	0.95 (0.78–0.97)
TS2	1	47	34	125	188	0.04	0.64	1.51 (1.33–1.60)	1.19 (1.07–1.21)	1.88 (1.84–1.92)
	2	47	42	136	204	0.03	0.66	1.53 (1.46–1.66)	1.37 (1.28–1.46)	1.69 (1.60–1.69)
TS3	1	484	93	469	835	0.09	0.24	0.96 (0.93–1.13)	0.94 (0.90–1.00)	0.97 (0.94–1.04)
	2	484	74	468	833	0.08	0.28	1.24 (1.11–1.28)	1.18 (1.11–1.19)	1.42 (1.33–1.48)
	3	484	66	442	787	0.08	0.25	1.06 (1.02–1.15)	0.80 (0.77–0.89)	1.26 (1.21–1.43)
SA	1	75	66	188	254	0.06	0.60	1.78 (1.58–2.00)	1.34 (1.29–1.47)	1.88 (1.79–2.06)
	2	75	70	223	302	0.19	0.29	0.86 (0.83–0.95)	0.75 (0.72–0.81)	0.88 (0.76–0.91)

The datasets are from the Inner Moray Firth (NS1), the North Sea (NS2–NS8), the Timor Sea (TS1–TS3) and offshore Brazil (SA). Horizons for individual datasets are listed in order of increasing age. Maximum fault throws are given in milliseconds (ms) and metres (m). Population slopes (for all faults (m), synthetic faults (m_s) and antithetic faults (m_a)) are reported as best estimates, with the minimum and maximum estimates in parentheses.

the growth curve for the backstripped Inner Moray Firth 2D population. A negative correlation between m_s and total strain for synthetic fault sets is observed (Fig. 7b); however, there is no correlation between these parameters for antithetic fault sets (Fig. 7c). However, when the m values for antithetic (m_a) and synthetic (m_s) populations are plotted against the component of the total strain accommodated by the individual fault sets, there is a well defined negative correlation between m and strain (Fig. 7d). There is a good correlation between polarity and m_a (Fig. 8a), but no relationship between polarity and m_s (Fig. 8b)

The data, therefore, suggest that the primary control on m values for synthetic and antithetic sub-populations is the strain accommodated by the individual sub-populations (Fig. 7d), again demonstrating the tendency for strain to localise onto larger faults during the growth of fault systems. The correlation between m_s and total strain (Fig. 7b) also reflects progressive strain localisation. The lack of a correlation between total strain and m_a (Fig. 7c) is not surprising when we consider the growth history of the Inner Moray Firth area. The antithetic faults in that area became inactive early in the growth of the fault system so that m_a was fixed at a relatively early stage and was unaffected by the subsequent increase in strain. For this area, therefore, the main control on m_a is not the present day total strain but the strain when the antithetic faults became inactive. The absence of a general relationship between m_a and total strain, for the other datasets studied, therefore indicates the tendency for antithetic fault populations to die over some time interval during the growth of the fault system. That the primary control on m_a is the strain accommodated by antithetic faults prior to their death is consistent with a positive correlation between polarity and m_a (Fig. 8a) and the absence of a relationship with m_s (Fig. 8b). If an antithetic fault set dies early in the growth of a fault system then it would be expected to have a relatively high population slope (Fig. 7d) and the fault system would eventually develop a high polarity, i.e. the final strain on the synthetic faults would be much larger than that on the antithetic faults. The population slope for synthetic faults appears to be independent of the timing of the death of the antithetic population. Irrespective of the precise controls on m_a and m_s we suggest that an antithetic population can be regarded as a lower strain equivalent of its synthetic sister population. Antithetic and synthetic populations are therefore interpreted to represent two 'snap-shots' in the strain evolution of initially similar populations.

3.2. Strain vs. polarisation

The progressive localisation of strain onto synthetic faults during extension might be expected to produce a positive correlation between strain and polarity; such a relationship is not observed for our data (Fig. 9). The lack of a correlation between these two parameters is attributed to the effect of pre-existing structure, i.e. to reactivation of

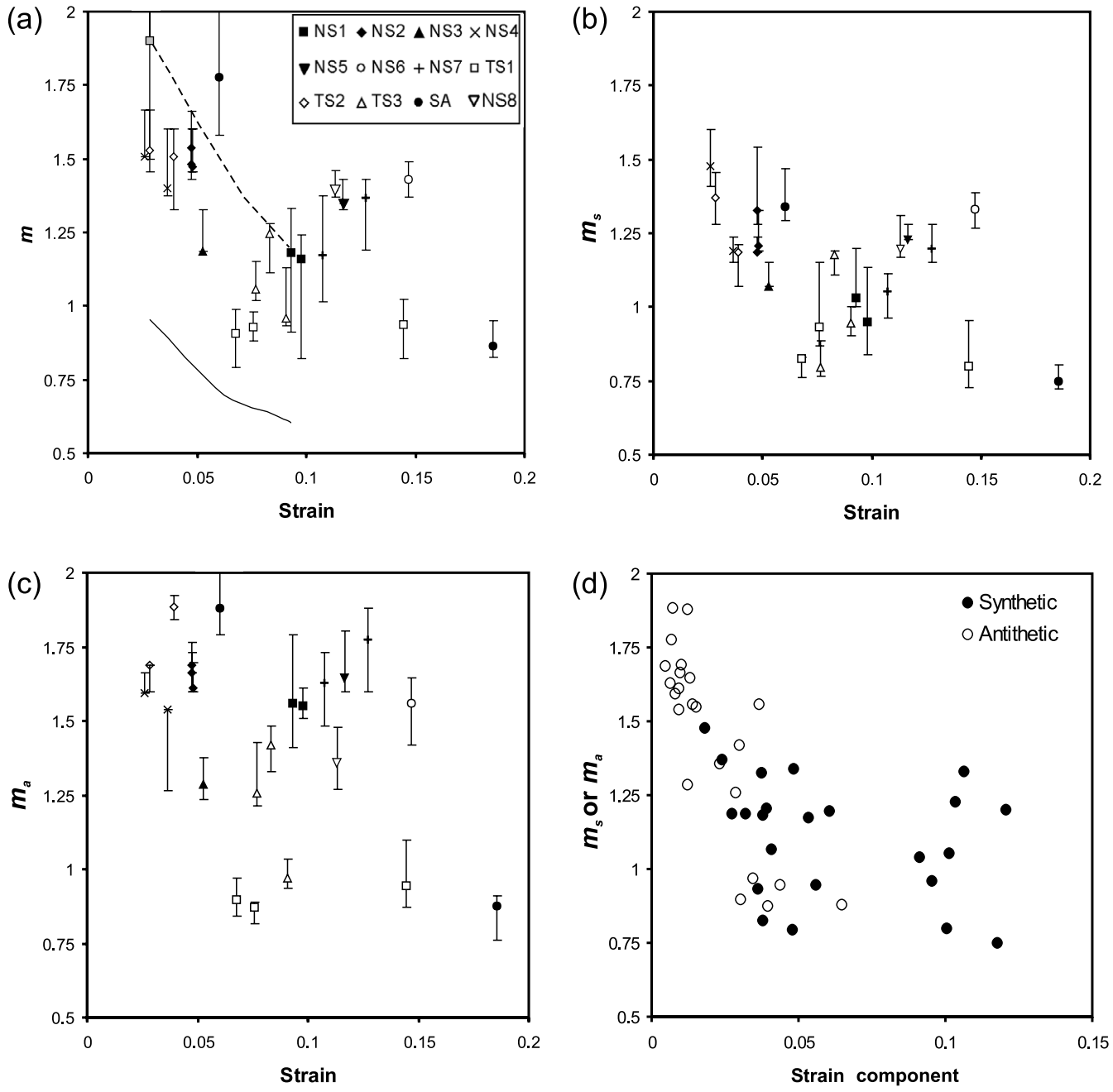

Fig. 7. Throw population slope (m) vs. total strain for (a) all faults, (b) synthetic faults and (c) antithetic faults for fault systems listed in Table 2. (d) Population slope for synthetic and antithetic faults plotted against the strains accommodated on the individual sub-populations. The m vs. strain growth curve for the Inner Moray Firth area determined for the 1D backstripped populations (Fig. 3) is shown in (a) (solid line). An approximately equivalent 2D growth curve is also drawn (dotted line). This 2D growth curve is constrained at either end by the present day population and the population restored to the earliest syn-faulting horizon (see Fig. 2d) and is interpolated at intermediate points from the 1D curve.

earlier formed faults at depth. The possible reactivation geometries and their likely effects on a strain/polarity relationship are illustrated in Fig. 10. Where a basin forms at approximately the same location as a pre-existing basin in the basement, then faults on the margins of the newly formed basin will become polarised in the same direction as the basement faults (Fig. 10c). Many of the faults in the newly formed basin will reactivate underlying structures and the newly formed fault system will become polarised sooner than if it formed in an area of previously undeformed crust (Fig. 10c). For example, in the SA area (Fig. 6a) there have been two phases of extension, one prior to and one following deposition of Horizon 1. Both extensional phases are due to eastward sliding above a salt detachment beneath Horizon 2. The strain on Horizon 2 is larger than that on Horizon 1 (Fig. 9) while the later horizon is more strongly polarised than Horizon 2. The later fault system therefore reactivated the earlier polarised system and was strongly

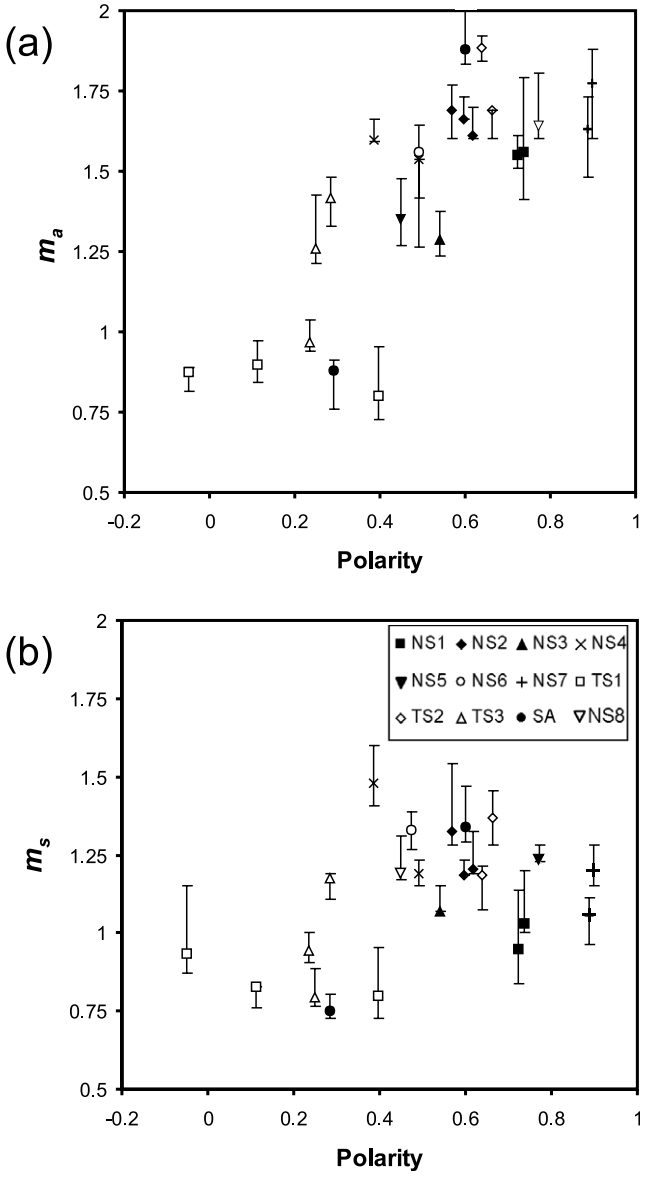

Fig. 8. Slope of (a) antithetic and (b) synthetic population slopes vs. polarity.

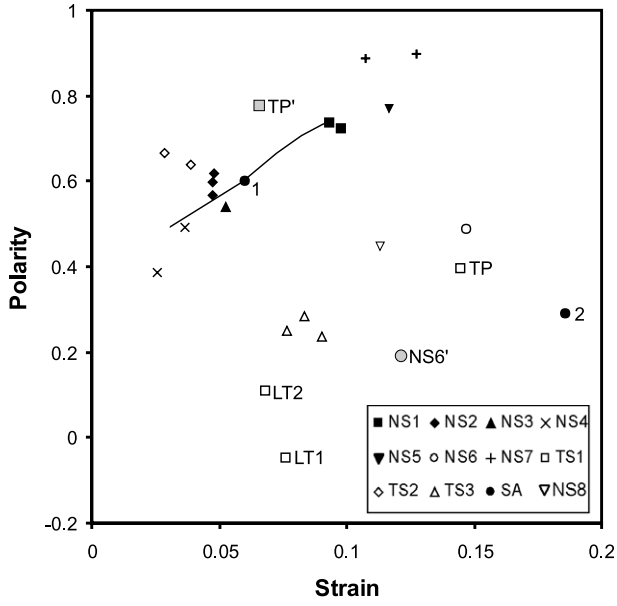

Fig. 9. Plot of fault system polarity vs. strain including growth curve (solid line) derived for the Inner Moray Firth area (Fig. 4). Horizons 1 and 2 for the SA dataset and the Lower Tertiary (LT) and Top Permian (TP) horizons for the TS1 dataset are labelled and discussed in the text. The datapoint labelled TP′ is for the Top Permian horizon following Late Jurassic faulting and prior to Tertiary reactivation (see text). The point labelled NS6′ is for the NS6 dataset but for an enlarged area that spans the axis of the Viking Graben (see text and Fig. 6c).

polarised from the outset as illustrated in Fig. 10c. The same is true for the TS2 area, for which two horizons deposited between two phases of extension are shown in Fig. 9, but the reverse of this situation is seen for the TS1 area (Fig. 6b). The TS1 area, which has been described in detail in Meyer et al. (2002), lies to the NW of a Late Jurassic–Early Cretaceous basin, but to the SE of a Tertiary basin, and the sense of fault polarisation within the TS1 area has therefore, reversed (Fig. 10d). For horizons deposited prior to the first phase of faulting, i.e. the Top Permian horizon (Fig. 6b), the polarity developed in the earlier faulting phase (0.75; see Fig. 9) would have decreased during Tertiary reactivation and the present day polarity (~0.4) is the net of the two faulting phases. For horizons deposited between the two faulting periods, i.e. Lower Tertiary 1 and 2 (Fig. 6b), initial reactivation of the Late Jurassic faults would have favoured the SE dipping Tertiary fault set. However, as Tertiary extension progressed, the fault system would have become polarised towards the newly formed basin with the NE dipping faults becoming progressively more important so that the net polarity is close to zero (Fig. 9). The TS3 horizons are also deposited in the same setting as the Lower Tertiary horizons in TS1, i.e. between two oppositely polarised faulting phases.

On the plot of strain vs. polarity, most of the North Sea data lie on or adjacent to the growth curve for the Inner Moray Firth area (Fig. 9). As described previously, this trend, when extrapolated to zero strain, intersects the polarity axis at a value of ca. 0.3 indicating that these North Sea areas were polarised very early and at strains less than 0.02. This early polarisation may be due to reactivation of earlier (possibly Triassic) fault systems or may indicate a more general trend for fault systems in ‘virgin’ ground, i.e. fault systems might become polarised early even in the absence of pre-existing structure. Therefore, while the lack of a simple relationship between strain and polarity data is explained by the presence of pre-existing structure at depth, uncertainty in deep structure for many areas, and in particular the North Sea, precludes definition from our data of a general polarisation trend for fault systems in virgin ground from our data. It is possible that only Horizon 2 from the SA dataset lies on such a trend.

The absence of a clear relationship between polarity and

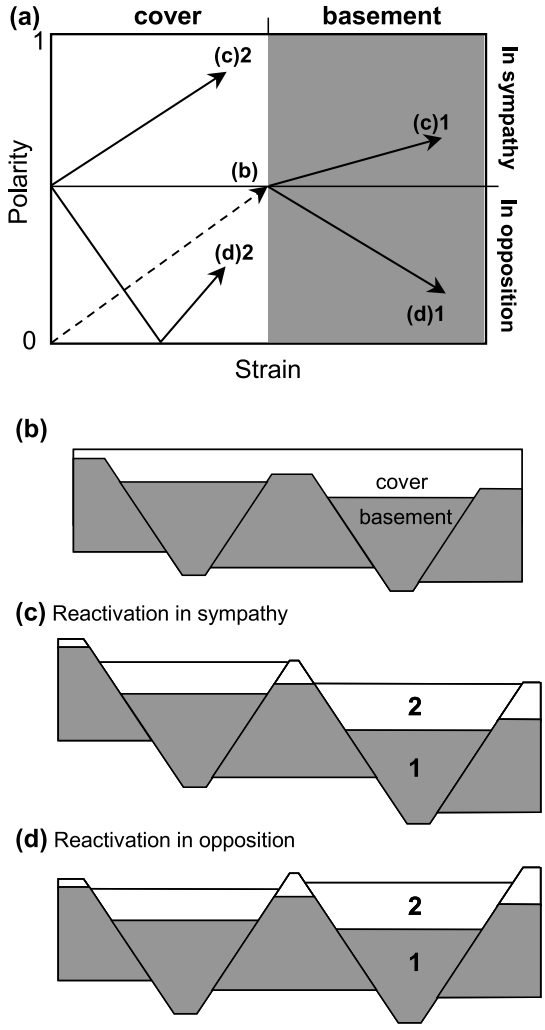

Fig. 10. Schematic diagram showing how the relationship between strain and fault polarity is masked by reactivation of pre-existing faults. (a) Shows the relationship between strain and polarity measured in basement (1) and cover (2) fault systems for different fault reactivation geometries. An initial fault system evolves along the dashed line in (a) resulting in a polarised fault pattern that is buried by post-rift sediments (b). Faults that are active during a later phase of extension may be polarised (c) in sympathy with or (d) in opposition to the earlier formed fault system, giving rise to different polarity/strain ratios in the basement and cover. The fault system polarity in the cover is assumed to be the same as that in the basement at the onset of reactivation i.e. 0.5. The growth curve for a cover sequence reactivated in opposition to the basement fault system d2 in (a) rebounds from the abscissa when cover sequence offsets on the faults that dip to the left become greater than those dipping to the right; in a more complex fault pattern than that shown, negative values of polarity may occur.

strain for several datasets (Fig. 9) precludes demonstrating that fault system polarity generally increases as fault systems evolve, as was demonstrated for the backstripped Moray Firth dataset (Fig. 4). Evidence for such a tendency is, however, provided by a positive correlation between polarity and the difference in slope between synthetic and antithetic sub-populations (Fig. 11). Given the strong correlation between the slope of synthetic and antithetic sub-populations and the strains that they accommodate

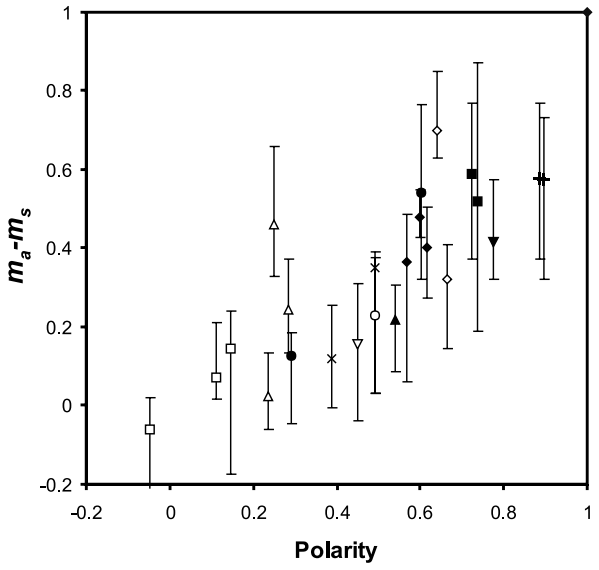

Fig. 11. Difference in population slope between antithetic and synthetic sub-populations vs. polarity.

(Fig. 7d), a relationship between difference in slope and difference in strain is to be expected. However, there is no correlation between difference in slope and total strain. These observations are consistent with a model for the evolution of fault populations as illustrated on the strain vs. slope growth curve for fault sub-populations shown in Fig. 12. In this model, fault systems evolve by progressive decrease in the slope of antithetic and synthetic populations. At some point in the growth of the fault system the antithetic faults become subordinate or completely inactive. If this occurs early in the growth of the fault system then the fault system is strongly polarised with a large difference in sub-population slopes (circles in Fig. 12). If the system becomes polarised late (squares in Fig. 12) then there is little or no difference between the slopes of the two sub-populations. The two fault systems illustrated in Fig. 12 accommodate

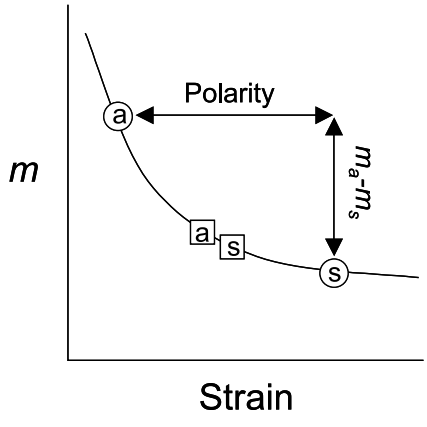

Fig. 12. Schematic plot of sub-population slope against strain accommodated on the individual sub-populations showing an idealised growth curve based on Fig. 7d. Antithetic (a) and synthetic (s) sub-populations are shown for two fault systems, shown by squares and circles, with the same total strain.

the same total strain but the slopes of the component sub-populations are different. In terms of relating fault population slopes to fault system maturity there are therefore two primary controls, the total strain and the polarity. We suggest, therefore, that fault system polarity increases with fault system evolution but is not simply related to the usual measure of maturity, i.e. strain, due to complications imposed by, for example, fault system reactivation.

4. Discussion

4.1. Sampling artefacts in power-law populations

In order to establish that the data trends described in the previous section are a reflection of geological processes rather than artefacts of sampling we have investigated these trends for artificial power-law fault populations. When a power-law population of fault throws is sub-divided randomly into two sub-populations of unequal size and these sub-populations are assigned to be synthetic or antithetic based on the size of the largest fault, there is no systematic difference in the slopes of the two sub-populations. In such an exercise, the power-law regression fitted to each artificial sub-population does not include the largest fault in the sub-population as this fault may not lie on the power-law trend defined by the majority of the data but can strongly bias the regression. Excluding the largest fault replicates what is done in practice when fitting straight lines to power-law trends. For our natural fault data however, m_a is always higher than m_s, with one exception, demonstrating that the antithetic and synthetic sub-populations are not arbitrary sub-samples of a single population.

4.2. Sampling and scaling

Scale-bound fault systems, for example populations of faults that offset the entire crust (Jackson and White, 1989), may be non-power-law and therefore display strain homogeneity at a particular scale, e.g. the crustal scale. In the absence of mechanical constraints on scaling, tectonic fault systems generally obey power-law scaling systematics and are therefore characterised by heterogeneous strains at all scales of observation. For the areas studied here, strain magnitude will therefore differ from our estimated values on scales both smaller and larger than that of the study area. The strain estimates are therefore only appropriate to the scale on which they are measured. Trends within our dataset, such as those in Fig. 7a, could be the result of strain heterogeneity in power-law systems if there existed systematic relationships between, for example, sample area or number of faults and either strain or power-law exponent. There are no such systematic relationships within our dataset and we conclude that the trends we observe are real trends defined for the scale range we have examined rather than an artefact reflecting the scaling properties of power-law systems.

Strain estimates for the fault populations presented were calculated, using Eq. (2), from seismically resolvable faults. However, sub-resolution faults may accommodate a significant strain because for power-law fault size populations the proportion of strain on sub-resolution faults increases with increasing population slope. To examine the possible impact of sub-resolution strain on the conclusions in this article we have estimated the strain in each dataset on faults with displacements greater than 10 cm and for a range of fault displacement:length ratios. Although inclusion of sub-resolution strain causes a narrowing of the range of strain estimates in, for example, Fig. 7, the data trends observed are maintained for the range of exponents typical of the relationship between fault displacement and length for normal faults, i.e. 1–2 (Watterson, 1986; Cowie and Scholz, 1992; Dawers et al., 1993).

The fault populations presented in this article demonstrate a progressive decrease in fault population slope with strain. We are not concerned here with the detailed character of each individual fault population curve, instead the estimated fault population slopes are taken as a measure of the relative numbers of small and large faults within a population; this approach is sufficiently accurate for the purposes of this article. In particular, we have not addressed the issue of whether or not fault populations depart from power-law scaling at high strains. A cursory inspection of the population curves in Fig. 5 suggests that power-laws at high strains (e.g. NS6) are as well defined as those at lower strains (e.g. NS4). A rigorous test of the change in population scaling with strain would require that the data are examined in terms of frequency, rather than cumulative frequency, and that populations of active faults are studied, i.e. for multiple horizons within a syn-sedimentary sequence, which the data do not allow. Such an approach was adopted by Walsh et al. (2003) in their analysis of the Inner Moray Firth area where they recognised the development of a distinct non-power-law tail at large lengths during the later stages of fault system evolution.

When estimating polarisation of a fault system it is crucial that an appropriate area is selected. An appropriate area is one that lies within a single polarity domain at the scale of observation. For example, if the sample area is the entire width of a symmetrical basin then the total polarity of the fault system, as defined here, would be close to zero. Including data from both margins of a graben together would therefore preclude any definition of a relationship between strain and polarity and between m and strain for the component fault dip directions (Fig. 7d), as antithetic faults on one margin are synthetic on the other margin. A correlation between the total strain and m would, however, be unaffected (Fig. 7a). Fig. 5c is a cross-section from the NS6 area. This dataset covers a significant area of the Viking Graben, North Sea. Although the greater part of the area covers the eastern flank of the graben, it also

includes part of the western flank. The predominant fault dip direction is reversed across the floor of the graben. The effect of including the faults from the western flank of the graben is to greatly reduce the polarity from 0.47 for the eastern flank to <0.2 as shown in Fig. 9.

The polarity measures derived in the previous sections are applicable to the scale on which they are measured. Within individual areas there are likely to be subareas within which the polarisation of the fault system will be the reverse of that of the area as a whole. For example, within the subarea of the Inner Moray Firth outlined in Fig. 1a, the majority of faults and the largest faults dip in opposition to the largest faults within the system as a whole. If sufficient data were available for this sub-area we suggest that it would yield similar relationships between strain and m values as the area as a whole, but with a reversal of the sense of polarity. The faults within this area of the map became inactive relatively early in the growth of this fault system due to localisation of strain onto the larger south-east dipping faults and the accompanying polarisation of the fault system in a southerly direction. It may also be true that on a scale larger than that of the available dataset, the system is polarised in the north-easterly direction onto faults that are larger and were active longer than those in the study area. We suggest, therefore, that as strain localisation occurs on progressively larger scales during the evolution of a fault system, polarisation also occurs on increasingly larger scales. Nicol et al. (1997) have shown that the relative displacement rates of faults within fault systems are established very early during extension so that large faults were always moving faster than small faults. This observation, combined with a recently proposed model for fault growth (Walsh et al., 2002) in which the majority of faults grow to close to their final lengths very rapidly, suggests that the locations of large, ultimately basin bounding faults can be predestined from a very early stage. In such a model, strain localisation and fault system polarisation occur during amplification of displacements on structures that were established at the very early stages of rifting. In this sense, the locations of graben axes are controlled by the fault localisation history but this history is either determined very early or from the outset, perhaps by deep crustal structure.

5. Conclusions

1. The slope of fault throw populations decreases as strain increases on extensional fault systems due to the progressive localisation of strain onto larger faults and the death of smaller faults.
2. The slopes of antithetic and synthetic sub-populations decrease with the strains they accommodate individually.
3. The slope of a synthetic fault sub-population is lower than that of an antithetic population in the same area. This difference in slope increases with increasing polarity.
4. Antithetic fault sub-population slopes are higher than synthetic population slopes because the antithetic faults died earlier and at lower strains than the synthetic faults. The slopes of antithetic sub-populations are dependent on the strain they accumulated by the time they became inactive, as reflected in the fault system polarity, rather than the total strain accommodated by the whole fault system.
5. The slopes of synthetic sub-populations decrease with increasing strain but are independent of fault system polarity.
6. There is no general relationship between the polarity of a fault system and the strain that it accommodates. The absence of such a relationship is attributed to the effects of underlying structure and the dip direction of pre-existing faults in the basement. For a single dataset in which fault system growth can be reconstructed, polarity increased as strain accumulated.
7. Strain localisation and fault system polarisation are expected to occur on progressively larger scales with increasing strain.

Acknowledgements

We thank other members of the Fault Analysis Group for useful discussion. The work was partly funded by Enterprise Ireland Grant SC/00/041. Randall Marrett and an anonymous reviewer are thanked for their helpful reviews.

References

Childs, C., Walsh, J.J., Watterson, J., 1990. A method for estimation of the density of fault displacements below the limits of seismic resolution in reservoir formations. In: Buller, A.T., Berg, E., Hjelmeland, O, Kleppe, J., Torsæter, O., Aasen, J.O. (Eds.), North Sea Oil and Gas Reservoirs II. Graham and Trotman, London, pp. 309–318.

Childs, C., Easton, S.J., Vendeville, B.C., Jackson, M.P.A., Lin, S.T., Walsh, J.J, Watterson, J., 1993. Kinematic analysis of faults in a physical model of growth faulting above a viscous salt analogue. Tectonophysics 228, 313–329.

Cladouhos, T.T., Marrett, R., 1996. Are fault growth and linkage models consistent with power-law distributions of fault lengths? Journal of Structural Geology 18, 281–294.

Cowie, P.A., 1998. A healing-reloading feedback control on the growth rate of seismogenic faults. Journal of Structural Geology 20, 1075–1087.

Cowie, P.A., Scholz, C.H., 1992. Displacement–length scaling relationship for faults: data synthesis and discussion. Journal of Structural Geology 14, 1149–1156.

Cowie, P.A., Sornette, D., Vanneste, C., 1995. Multifractal scaling properties of a growing fault population. Geophysical Journal International 122, 457–469.

Dawers, N.H., Anders, M.H., 1995. Displacement–length scaling and fault linkage. Journal of Structural Geology 17, 607–614.

Dawers, N.H., Anders, M.H., Scholz, C.H., 1993. Fault length and displacement: scaling laws. Geology 21, 1107–1110.

Fossen, H., Hesthammer, J., 1998. Structural geology of the Gullfaks Field,

northern North Sea. In: Coward, M.P., Daltaban, T.S., Johnson, H. (Eds.), Structural Geology in Reservoir Characterisation Special Publication of the Geological Society, vol. 127, pp. 231–261.

Higgs, W.C., McClay, K.R., 1993. Analogue sandbox modelling of Miocene extensional faulting in the Outer Moray Firth. In: Williams, G.D., Dobb, A. (Eds.), Tectonics and Seismic Sequence Stratigraphy Special Publication of the Geological Society, vol. 71, pp. 141–162.

Ishikawa, M., Otsuki, K., 1995. Effects of strain gradients on asymmetry of experimental normal fault systems. Journal of Structural Geology 17, 1047–1053.

Jackson, J.A., White, N.J., 1989. Normal faulting in the upper continental crust: observations from regions of active extension. Journal of Structural Geology 11, 15–36.

Kakimi, T., 1980. Magnitude–frequency relation for displacement of minor faults and its significance in crustal deformation. Bulletin of the Geological Survey of Japan 31, 467–487.

Marrett, R., Allmendinger, R.W., 1991. Estimates of strain due to brittle faulting: sampling of fault populations. Journal of Structural Geology 13, 735–738.

Marrett, R., Allmendinger, R.W., 1992. Amount of extension on 'small' faults: an example from the Viking Graben. Geology 20, 47–50.

Meyer, V., Nicol, A., Childs, C.C., Walsh, J.J., Watterson, J., 2002. Progressive localisation of strain during the evolution of a normal fault population. Journal of Structural Geology 24, 1215–1231.

Nicol, A., Walsh, J.J., Watterson, J., Underhill, J.R., 1997. Displacement rates of normal faults. Nature 390, 157–159.

Petersen, K., Clausen, O.R., Korstgård, J.A., 1992. Evolution of a salt-related listric growth fault near the D-1 well, block 5605, Danish North Sea: displacement history and salt kinematics. Journal of Structural Geology 14, 565–577.

Pickering, G., Bull, J.M., Sanderson, D.J., 1995. Sampling power–law distributions. Tectonophysics 248, 1–20.

Ranalli, G., 1977. Correlation between length and offset in strike-slip faults. Tectonophysics 37, T1–T7.

Schlische, R.W., Young, S.S., Ackerman, R.V., 1996. Geometry and scaling relations of a population of very small rift-related normal faults. Geology 24, 683–686.

Scholz, C.H., Cowie, P.A., 1990. Determination of total strain from faulting using slip measurements. Nature 346, 837–839.

Stewart, S.A., Argent, J.D., 2000. Relationship between polarity of extensional fault arrays and presence of detachments. Journal of Structural Geology 22, 693–711.

Underhill, J.R., 1991a. Controls on Late Jurassic seismic sequences, Inner Moray Firth, UK North Sea: a critical test of a key segment of Exxon's original global cycle chart. Basin Research 3, 79–98.

Underhill, J.R., 1991b. Implications of Mesozoic–Recent basin development in the western Inner Moray Firth, UK. Marine and Petroleum Geology 8, 359–369.

Walsh, J.J., Watterson, J., 1988. Analysis of the relationship between the displacements and dimensions of faults. Journal of Structural Geology 10, 239–247.

Walsh, J.J., Watterson, J., Yielding, G., 1991. The importance of small-scale faulting in regional extension. Nature 351, 391–393.

Walsh, J.J., Watterson, J., Yielding, G., 1994. Determination and interpretation of fault size populations: procedures and problems. In: Aasen, J.O., Berg, E., Buller, A.T., Hjelmeland, O., Holt, R.M., Kleppe, J., Torsæter, O. (Eds.), North Sea Oil and Gas Reservoirs III. Kluwer, London, pp. 141–155.

Walsh, J.J., Nicol, A., Childs, C., 2002. An alternative model for the growth of faults. Journal of Structural Geology 24, 1669–1675.

Walsh, J.J., Childs, C., Imber, J., Manzocchi, T., Watterson, J., Nell, P.A.R., 2003. Strain localisation and population changes during fault system growth. Journal of Structural Geology 25, 1897–1911.

Watterson, J., 1986. Fault dimensions, displacements and growth. Pure and Applied Geophysics 124, 365–373.

Watterson, J., Walsh, J., Gillespie, P.A., Easton, S., 1996. Scaling systematics of fault sizes on a large scale range fault map. Journal of Structural Geology 18, 199–214.

Wojtal, S.F., 1994. Fault scaling laws and the temporal evolution of fault systems. Journal of Structural Geology 16, 603–612.

Wojtal, S.F., 1996. Changes in fault displacement populations correlated to linkage between faults. Journal of Structural Geology 18, 265–279.

Yielding, G., Needham, T., Jones, H., 1996. Sampling of fault populations using sub-seismic data: a review. Journal of Structural Geology 18, 135–146.